Rare Metal Materials and Engineering
Volume 52, Issue 7, July 2023
Available online at www.rmme.ac.cn

Science Press

Cite this article as: Qi Yingnan, Liu Zongde, Xie Ruixiang, et al. Corrosion Characteristics of Cu-Mn Cladding Layers with Different Mn Contents[J]. Rare Metal Materials and Engineering, 2023, 52(07): 2353-2363.

ARTICLE

Corrosion Characteristics of Cu-Mn Cladding Layers with Different Mn Contents

Qi Yingnan, Liu Zongde, Xie Ruixiang, Ma Herong, Ning Huaqing

Key Laboratory of Power Station Energy Transfer Conversion and System, Ministry of Education, North China Electric Power University, Beijing 102206, China

Abstract: To investigate the corrosion characteristics and anti-fouling properties of Cu-Mn cladding layers with different Mn contents, the laser cladding technique was used to prepare Cu-Mn cladding layers with homogeneous composition and low dilution rate. Electrochemical tests, salt spray corrosion experiments, corrosion morphology observations, and copper ion release tests were conducted to investigate the corrosion characteristics of Cu-Mn cladding layers with different Mn contents in 3.5wt% NaCl solution. The effect of Mn on corrosion products and copper ion release rate was particularly studied. Results show that the corrosion resistance of cladding layers is decreased with increasing the Mn content during the electrochemical tests. In the salt spray corrosion experiments, the corrosion degree of the Cu-Mn cladding layer is deepened with increasing the Mn content, and the average mass loss is increased. The corrosion morphology of cladding layers after electrolytic corrosion was observed. Compared with those of Cu-Mn cladding layer with low Mn content, the corrosion products generated from Cu-Mn cladding layer with high Mn content have more sparse structure, the number of crack holes is larger, and the corrosion products are easier to peel off. In the copper ion release test, all cladding layers can inhibit the growth of sea creatures. The higher the Mn content, the greater the copper ion release rate, presenting great application potential in anti-fouling materials.

Key words: Cu-Mn alloy; laser cladding; electrochemical; salt spray corrosion; corrosion morphology; copper ion

Copper has been extensively used in different fields. With the continuous development of science and technology, higher requirements have been proposed for the copper and copper alloys in the modern industry[1–2]. In the complex marine environment, copper alloys have good resistance against the seawater corrosion and adhesion of aquatic organisms, therefore providing specific anti-fouling effects as ship material[3–4]. The anti-fouling ability of copper alloys can be affected by the corrosion rate in seawater, the nature of corrosion product on surface, and the adhesion degree[5–8]. With prolonging the exposure time, the anti-fouling performance of normal copper alloys and pure copper declines: a dense layer containing alkali copper chloride, alkali copper carbonate, and other corrosion products is gradually formed, and the continuous deposition of these corrosion products leads to a significant reduction in the precipitation rate of copper ions, which seriously affects the anti-fouling effect[9–12]. It is reported that only when the corrosion products on the copper alloy surface are loose and contain cracks, the corrosion products will peel off under the shear force at a specific flow rate, thereby achieving the self-polishing effect and long-term prevention against sea life adhesion[13–14].

Cu-Mn alloys are often used in marine systems due to their excellent strength and damping properties. As reported in Ref.[15], a certain amount of Mn is doped into cladding hulls and cabins of copper alloys to enhance their strength. It is concluded that Mn plays a crucial role in enhancement of mechanical properties[16], phase stability[17–18], and oxidation resistance[19]. However, the effect of Mn addition on the corrosion properties of copper alloys has rarely been researched, particularly the resistance against seawater corrosion and fouling. Moreover, the effect mechanism of Mn addition on the corrosion and fouling resistance of copper

---

Received date: January 11, 2023
Foundation item: Study Project of Galvanic Corrosion Behavior and Protection Technology of Dissimilar Structural Materials in South China Sea Environment (61409220202)
Corresponding author: Liu Zongde, Ph. D., Professor, Key Laboratory of Power Station Energy Transfer Conversion and System, Ministry of Education, North China Electric Power University, Beijing 102206, P. R. China, Tel: 0086-10-61772812, E-mail: lzd@ncepu.edu.cn

alloys is still obscure. The corrosion characteristics of Cu-Mn coatings have been widely researched[20–21]: by changing the corrosion medium, electrochemical potential, and other conditions, the Cu-Mn cladding layer can be selectively corroded. Thus, the porous corrosion product can be obtained. Zhang et al[22] conducted corrosion experiments on the surface of Cu-Ni alloys with different Mn contents in 3.5wt% NaCl solution and found that the alloy with low Mn content has better corrosion resistance. Pardo[23] and An[24] et al both pointed out that Mn addition is beneficial to the pitting corrosion resistance. However, the effect of Mn addition on the corrosion characteristics of copper alloys, especially on the surface corrosion products, has rarely been investigated.

Laser cladding technique contains the rapid cladding and solidification of metal powders through the high-energy-density laser beam, and it can achieve well-formed coatings with low element dilution, no cracks, and good metallurgical bonding with the substrate[25–26]. Compared with other processing methods, the Cu-Mn cladding layers produced by laser cladding technique have higher bonding strength as well as more homogeneous and stable organization. Additionally, the composition of cladding layer can be sightly influenced[27–29].

In this research, the Cu-Mn cladding layers with different Mn contents were prepared on the base material by laser cladding technique. Through electrochemical tests, constant potential electrolytic acceleration, salt spray corrosion experiments, corrosion morphology characterization, and copper ion release rate monitoring, the effect of Mn content on the composition of surface corrosion products, corrosion product defects, and copper ion release rate was studied.

1 Experiment

Fig. 1 shows the schematic diagram of preparation process of Cu-Mn cladding layer with thickness of 1.2 – 1.5 mm on Q235 steel surface by Zhongke Zhongmei equipment with 3300 W fiber laser. The protective gas was Ar, and the powder feeding gas was N_2. The laser cladding parameters are shown in Table 1, and the chemical composition of the substrate and the three cladding layer specimens is shown in Table 2 and Table 3, respectively. Three specimens were machined into small cubes of 10 mm×10 mm×10 mm (the thickness of cladding layer was only 1.2 mm and the thickness of Q235 stainless steel was 8.8 mm). The working surfaces of three specimens were ground by 1500# sandpaper and polished by polishing paste with grain size of 0.5 μm. Finally, the specimens were rinsed by deionized water and ethanol, dried, and placed in a desiccator.

The CHI660E electrochemical workstation was used to test the open-circuit potential, kinetic potential polarization curves, and electrochemical impedance spectra of three specimens. The three-electrode system was used: the specimen was used as the working electrode, the saturated mercury electrode was used as the reference electrode, and the platinum sheet was used as the auxiliary electrode. The lower part of the capillary salt bridge was filled by saturated KCl agar solution, and the upper part was filled by saturated KCl solution. The saturated mercury electrode was placed in the saturated KCl solution, the distance between the capillary tip and the specimen surface was 3–5 mm, and the medium was 3.5wt% NaCl solution. The specimen was stabilized in the solution for 30 min and then tested at an open circuit potential (OCP) for 3600 s. The scanning range of the kinetic potential polarization curve was from −300 mV vs. OCP to 700 mV vs. OCP with scanning speed of 1 mV/s. The electrochemical impedance spectroscopy (EIS) test was performed at OCP with scanning frequency of 10^5–10^{-2} Hz and signal amplitude of 10 mV.

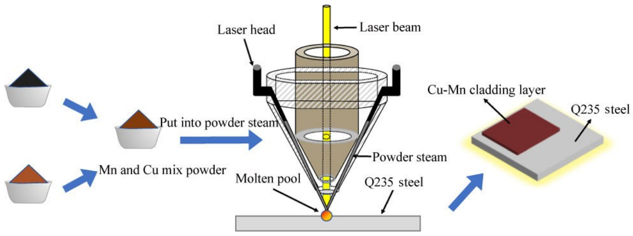

Fig.1 Schematic diagram of preparation process of Cu-Mn cladding layer by laser cladding with coaxial powder feed nozzle

Table 1 Experiment parameters of laser cladding for different Cu-Mn cladding layers

Specimen	Laser power/W	Scanning speed/$\text{cm}\cdot\text{s}^{-1}$	Overlapping
Mn3Cu	2450	6.67	0.6
Mn5Cu	2450	6.67	0.6
Mn7Cu	2450	6.67	0.6

Table 2 Chemical composition of Q235 stainless steel (wt%)

C	Si	Mn	P	S	Fe
0.22	0.35	0.14	0.045	0.05	Bal.

Table 3 Nominal composition of specimen powder (wt%)

Specimen	Mn	Cr	Ni	Cu
Mn3Cu	3	≤0.3	≤0.3	Bal.
Mn5Cu	5	≤0.3	≤0.3	Bal.
Mn7Cu	7	≤0.3	≤0.3	Bal.

The salt spray test was conducted according to GB/T 10125-2012 standard. The test solution was 3.5wt%±0.5wt% NaCl solution, and the pH value was 6.5 – 7.2. The temperature in the salt spray chamber was set at 35±1 °C, the temperature of the pressure drum was set at 45 °C, the humidity was more than 95%, the mist fall was 1 $\text{mL}\cdot\text{h}^{-1}\cdot\text{cm}^{-2}$, and the nozzle pressure was 70 kPa. In order to study the initial corrosion behavior of Cu-Mn cladding layer in the salt spray test, the specimens were taken out from the solution every 2 d for observation and mass loss tests, and the total duration was 12 d.

The corrosion morphologies were observed under accelerated electrolytic corrosion. The electrolytic acceleration potential was set as the potential corresponding to the maximum corrosion current of polarization curve during corrosion test. After corrosion tests, the electrolytic acceleration potential of the Mn3Cu, Mn5Cu, and Mn7Cu specimens was 0.01, 0.02, and 0.03 V, respectively. The electrolytic corrosion was conducted for 120 min. The Mn7Cu specimen suffered from more intense corrosion and it was selected to investigate the relationship between the electrolytic accelerated corrosion and corrosion duration. The time gradient was set as 120, 240, and 360 min. The temperature was 25 °C (room temperature), and the NaCl solution concentation was 3.5wt%. After experiments, the electrode was removed and used for corrosion morphology observation and corrosion product analyses.

The copper ion release rate test was conducted according to GB/T6824-2008 standard. Firstly, three large beakers of 1000 mL were prepared as storage tanks, and they were filled with 3.5wt% NaCl solution of 800 mL. Besides, three beakers of 200 mL were prepared as exudation tanks. The specimens were separately put into the storage tank at the beginning of the experiments. The specimens were taken out from the storage tank at specific time and put vertically into the exudation tank with 3.5wt% NaCl solution of 100 mL for the copper ion exudation experiment. The experiment apparatus was a self-designed rotation device, which could rotate clockwise with rotation rate of 45 r/min to simulate the seawater stirring. After rotation for 90 min, the specimens were taken out and put back into the storage tank. The exudate was taken into the centrifuge tube for further analyses, and the experiment was conducted for 45 d.

X-ray diffractometer (XRD, Rigaku D/Max-2400, Tokyo, Japan), scanning electron microscope (SEM, ZEISS EVO 18, Berlin, Germany; SEM, S-4800 HITACHI), and energy dispersive spectrometer (EDS, Bruker, Billerica, MA, USA) were used to analyze the surface morphology, element distribution, and phase composition of the corrosion product on the surface of Cu-Mn cladding layers with Mn addition of different contents after electrolysis accelerated corrosion. The thickness of corrosion product on the cross section of cladding layer and the corrosion products at different positions were analyzed.

2 Results and Discussion

2.1 OCP analysis

Fig. 2a shows OCP diagrams of Mn3Cu, Mn5Cu, and Mn7Cu specimens in 3.5wt% NaCl solution. OCP is related to the thermodynamic variation of material. The more positive the potential value, the higher the corrosion resistance of materials[30]. With prolonging the corrosion time, OCP of Mn3Cu, Mn5Cu, and Mn7Cu specimens is negatively shifted, and the shift difference becomes smaller. This phenomenon is due to the anode dissolution, which occurs under the action of Cl^- ions adsorbed on the specimen surface. The soluble chloride is formed according to the $Cu+2Cl^- \rightarrow CuCl^{2-}+e^-$ reaction. Subsequently, the reaction $2CuCl^{2-}+2OH^- \rightarrow Cu_2O+H_2O+4Cl^-$ occurs on the specimen surface, and the formed protective corrosion product film (Cu_2O) inhibits the anodic reaction on the surface to a certain extent[31–34]. The corrosion potential of three specimens is arranged as follows: Mn3Cu (−0.2167 V)>Mn5Cu (−0.2227 V)>Mn7Cu (−0.2338 V). Therefore, the higher the Mn content, the more negative the self-corrosion potential and the easier the occurrence of corrosion in seawater[31].

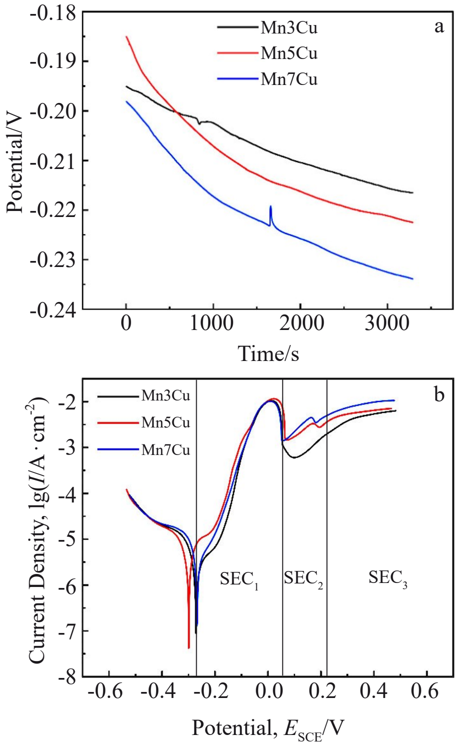

Fig.2 OCP results (a) and potentiodynamic polarization curves (b) of different Cu-Mn cladding layers in 3.5wt% NaCl solution

2.2 Dynamic potential polarization analysis

Fig.2b shows the Tafel curves of different Cu-Mn cladding layers in 3.5wt% NaCl solution. SEC_1 represents the active dissolution region, where Cu becomes Cu^+ and reacts with Cl^- in the solution. The related reactions may occur in this region, as follows:

$$Cu^+ + Cl^- \rightarrow CuCl \tag{1}$$

$$CuCl + Cl^- \rightarrow CuCl_2^- \tag{2}$$

The generated CuCl is insoluble in water. However, with increasing the polarization potential, CuCl is hydrolyzed to produce Cu_2O, and the following reaction occurs:

$$2CuCl + H_2O \rightarrow Cu_2O + 2HCl \tag{3}$$

In SEC_2 region, the oxide film can inhibit the Cl^- diffusion to the anode surface. Accordingly, the polarization current decreases. The polarization current can be increased with increasing the polarization voltage, leading to the partial dissolution of oxide film and producing Cu^{2+}, which corresponds to the SEC_3 region.

The polarization curves were treated through the Tafel cathodic extrapolation method, and Table 4 shows the fitting results of self-corrosion potentials and self-corrosion current

Table 4 Fitting electrochemical parameters of different Cu-Mn cladding layer specimens

Electrode specimen	Corrosion potential, E_{corr}/mV	Corrosion current density, I_{corr}/μA·cm^{-2}
Mn3Cu	−217	0.634
Mn5Cu	−223	0.679
Mn7Cu	−234	1.212

densities. It can be seen that the corrosion current density of Mn7Cu specimen is the largest of 1.212 μA·cm^{-2}, and that of Mn5Cu and Mn3Cu specimens is 0.679 and 0.634 μA·cm^{-2}, respectively. Therefore, with increasing the Mn content, the corrosion current is gradually larger and the corrosion potential becomes more negative, indicating that the corrosion resistance of Cu-Mn alloy is decreased with increasing the Mn content, which is consistent with the experiment results of self-corrosion potential. The corrosion current density of the Q235 steel at room temperature is about 2.6×10^{-5} A·cm^{-2} and its corrosion potential is about −0.6 V. The corrosion current densities of the three specimens in this research are all lower than 2.6×10^{-5} A·cm^{-2} and their corrosion potentials are all higher than −0.6 V, which indicates that the corrosion resistance of the cladding layer is better than that of the Q235 steel. Therefore, it can be concluded that the laser-cladding layer can effectively improve the corrosion resistance of alloys.

2.3 Corrosion current density at constant potential

Fig. 3 shows the current density curves during the electrolytic corrosion of copper-manganese alloy at constant potential. The coupling current densities of Mn3Cu, Mn5Cu, and Mn7Cu specimens are 1.14, 1.30, and 1.47 mA·cm^{-2}, respectively. Mn7Cu specimen has the largest coupling current density and Mn3Cu specimen has the smallest coupling current density. With prolonging the corrosion duration, the reaction of Cl$^-$ ions in solution is further intensified, suggesting that the oxide film on the surface of Cu-Mn alloys gradually reacts with Cl$^-$, and thereby the protective film gradually fails. It can be seen that the initial current densities of three specimens are high, and they gradually decrease to a constant value due to the new film generated on the specimen surface.

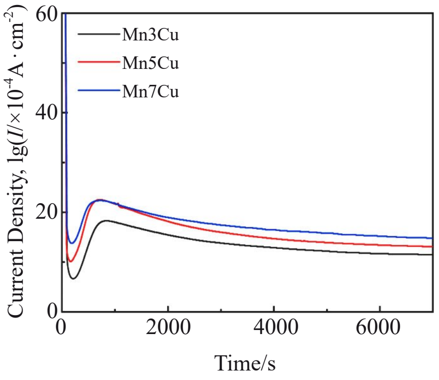

Fig.3 Current density curves under constant potential electrolytic corrosion of different Cu-Mn cladding layers

2.4 Impedance analysis

Fig. 4 shows the Nyquist plots and Bode plots of Mn3Cu, Mn5Cu, and Mn7Cu cladding layers in 3.5wt% NaCl solution. Fig. 4a shows that the Nyquist plots of different cladding layers all consist of a capacitive arc with a time constant and a nearly straight line. The capacitive arc exists in the low frequency region, which indicates that the electrode reaction is an interface reaction control process. Besides, the overall impedance is mainly composed of the impedance of the cladding layer. The slope of the straight line in the high frequency region is close to 1 (inclination angel of 45°), which infers that the electrode reaction rate in the high frequency region is controlled by the charge transfer process in the solution, and the impedance can be expressed as the solution impedance[35].

The radius of the capacitive arc reflects the magnitude of the charge transfer resistance, and the larger the impedance, the better the corrosion resistance of the electrode surface[36–37]. As shown in Fig. 4a, the radius of capacitive arc of Mn3Cu specimen is the largest, and Mn7Cu specimen has the smallest capacitive arc radius, which indicates that the corrosion reaction rate of Mn7Cu specimen is the fastest and that of Mn3Cu specimen is the slowest. According to Fig. 4b, the impedance |*Z*| of cladding layer reaction exists in the low frequency region (10^{-2} – 10^{1} Hz). It can be seen that the impedance is gradually decreased with increasing the Mn content, and the higher the impedance, the better the protection effect caused by the corrosion product (film) on the alloy surface. In the middle frequency region (10–10^3 Hz), the phase angle θ of the specimens reaches the maximum value.

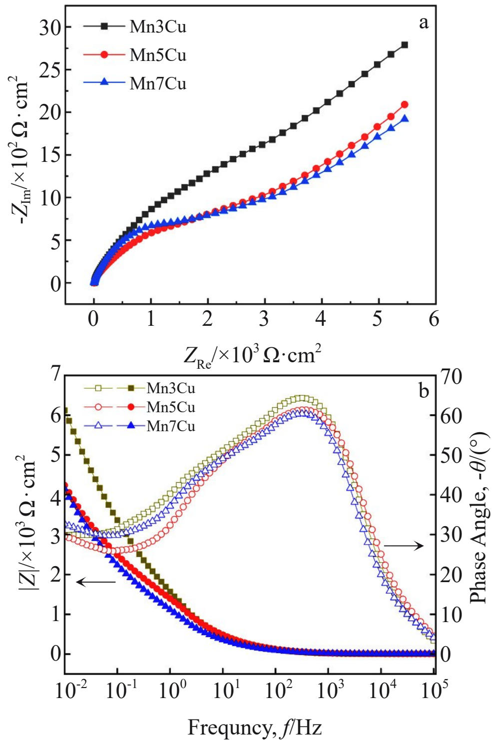

Fig.4 Nyquist plots (a) and Bode plots (b) of different Cu-Mn cladding layers after immersion in 3.5wt% NaCl solution

With decreasing the θ value to −90°, more and more corrosion products (film) are generated on the specimen surface, thereby forming a pure capacitive insulating layer, which improves the corrosion resistance of specimens. The maximum phase angle of Mn7Cn specimen is lower than that of other two specimens, indicating that its impedance caused by surface film is low, the ions can easily pass the protective film, and the Cu ion release rate is high. In the high frequency region (10^3–10^5 Hz), the phase angle becomes 0°, indicating that the main performance is dominated by solution impedance.

Fig. 5 shows the equivalent circuit diagram of Cu-Mn cladding layers with different Mn contents after corrosion in 3.5wt% NaCl solution, and the fitting data obtained from Bode plots (Zview software) are shown in Table 5. R_s denotes the solution resistance, CPE denotes constant phase angle element, and R_{ct} is the charge transfer resistance. The magnitude of the exponent n reflects the deviation degree of the electrode from the ideal electrode[38–39]. If n=0, the element is pure resistance (R); if n=1, the element is pure capacitance (C). The larger R_{ct} represents the slower charge transfer rate and the slower corrosion electrochemical process. The R_{ct} values of Mn3Cu and Mn5Cu specimens are close to each other, and that of Mn7Cu specimen is significantly smaller, indicating that after corrosion for a certain duration, the corrosion rate of Mn7Cu specimen is the fastest, and the Cu-Mn cladding layers with lower Mn contents have better corrosion resistance.

2.5 Salt spray test

After corrosion for 12 d, the surface appearances of different Cu-Mn cladding layers are shown in Fig. 6. The surface of cladding layers after salt spray corrosion has some red-black corrosion products and some patches of light green corrosion products. After comparing the cladding layers with different Mn contents, it is found that the corrosion degree of cladding layer is increased with increasing the Mn content. Besides, the corrosion products on the specimen surface gradually change with prolonging the corrosion duration. Therefore, it can be concluded that the corrosion degree of specimens is gradually increased with prolonging the corrosion duration, and a small amount of light green corrosion product gradually appears on the surface of Mn3Cu specimen. It can be seen that the Mn7Cu specimen suffers from the most serious corrosion after corrosion for 12 d.

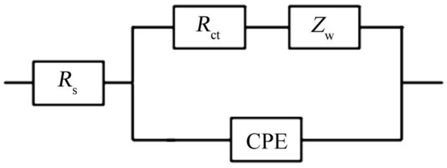

Fig.5 EIS equivalent circuit of Cu-Mn cladding layers with different Mn contents

Table 5 Fitting EIS equivalent circuit parameters of Cu-Mn cladding layer specimens with different Mn contents

Electrode specimen	R_s/Ω·cm²	R_{ct}/×10⁵ Ω·cm²	n
Mn3Cu	5.991	1.708	0.833
Mn5Cu	6.298	1.985	0.808
Mn7Cu	6.273	1.349	0.746

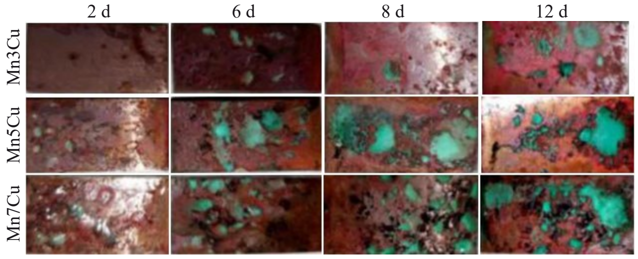

Fig.6 Surface appearances of Cu-Mn cladding layers with different Mn contents after salt spray corrosion for different durations

The corrosion rate of the specimen per unit area can be calculated based on the mass loss, as follows:

$$v = \frac{\left(M_0 - M_1\right)}{S} \tag{4}$$

where v is the corrosion rate (mm/a), M_0 is the average mass of the specimens before experiment (g), M_1 is the average mass of the specimens after descaling (g), and S is the surface area of the specimens (cm²).

Table 6 shows the mass loss per unit area of different Cu-Mn specimens after salt spray tests. The relationship between mass loss and corrosion duration of Cu-Mn cladding layers with different Mn contents is shown in Fig. 7. It is found that the mass loss is increased with increasing the Mn content, and the average mass loss of Mn7Cu specimen reaches 20.433 g/m² after salt spray corrosion for 12 d, which is about 1.20 times larger than that of Mn3Cu specimen.

Table 6 Average mass loss of salt spray specimens after corrosion for different durations (g/m²)

Specimen	2 d	4 d	6 d	8 d	10 d	12 d
Mn3Cu	2.547	4.901	7.418	11.658	12.462	17.153
Mn5Cu	2.746	6.277	11.129	13.827	15.751	18.581
Mn7Cu	2.840	7.021	12.370	15.076	17.649	20.433

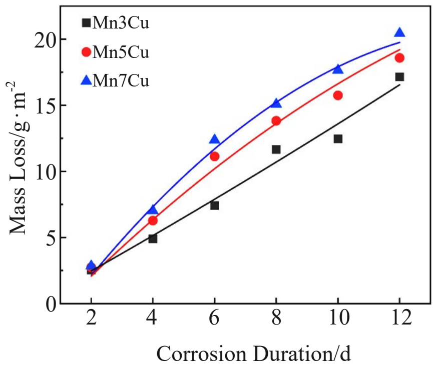

Fig.7 Relationship between mass loss and corrosion duration of Cu-Mn cladding layers with different Mn contents

As shown in Fig. 7, the fitting mass loss curves show the similar parabolic relationship. The corrosion rate of Mn7Cu specimen decreases in the late corrosion period, whereas that of Mn3Cu and Mn5Cu specimens slightly decreases, which may be due to the hindrance effect of the corrosion product (film) generated on the alloy surface. During the salt spray corrosion experiment, the corrosion rate of Mn7Cu specimen exceeds that of other two specimens, and the results indicate that the corrosion resistance of the cladding layer in the salt spray environment tends to decrease significantly with increasing the Mn content.

2.6 Corrosion morphology

Fig. 8 shows SEM morphologies of the surface corrosion products of different Cu-Mn cladding layers after electrolytic corrosion in 3.5wt% NaCl solution for 120 min. The Mn3Cu specimen after electrolytic corrosion for 120 min has dense morphology. Some flat gray flakes, a small number of cracks, and some pores appear on the surface of corrosion products. The Mn5Cu specimen morphology presents the surface cracking with some pitting areas after corrosion for 120 min. The corrosion of Mn5Cu specimen is more intense than that of Mn3Cu specimen, and a few areas of surface corrosion product already peel off, revealing the irregular white flake corrosion products with dense distribution on the specimen. The surface corrosion products produce many cracks and a small amount of shedding on the Mn7Cu specimen after corrosion for 120 min. It can be seen that there are mainly two kinds of corrosion products on the surface of Mn7Cu specimens: one is the loose bumpy corrosion product, and the other is the laminar corrosion product. Additionally, more holes can be observed in the shedding area of Mn7Cu specimen. Therefore, the higher the Mn content, the more intense the corrosion reactions. Mn7Cu specimen has the most intense corrosion reaction, so it was selected for further study of the corrosion characteristics of cladding layer.

Fig. 9 shows SEM morphologies of Mn7Cu specimen after corrosion for 240 and 360 min. It can be seen that under the same Mn content, with prolonging the electrolytic corrosion duration, the corrosion products have more cracks, and corrosion morphology is diversified. The longer the corrosion duration, the looser the surface corrosion products: the cracks and a small amount of shedding area gradually appear. The corrosion products in shedding area consist of lamellar stacked clusters and needle-like corrosion products. This phenomenon may be attributed to the severe corrosion, and the increasing defects cause the curl of corrosion products, forming the needle-like corrosion products.

Fig. 10 shows the cross-sectional corrosion products of different Cu-Mn cladding layers after accelerated corrosion at constant potential electrolysis in 3.5wt% NaCl solution. It can be seen that Mn3Cu and Mn5Cu corrosion products are sparse and have a small number of cracks and defects. Mn7Cu specimen shows an apparent delamination phenomenon, and its corrosion product is relatively loose with cracks and holes. The Mn7Cu corrosion products mainly consist of white flocculated products (area 2 and area 3 in Fig. 10d) and gray laminated products (area 1 in Fig. 10d). According to EDS analysis results of area 1 and area 2 (Table 7), along the corrosion product layer from the outside to the inside direction, the Cu content gradually increases, and the Mn element content gradually decreases. It is inferred that the Cu-related corrosion products are concentrated near the substrate surface, and the Mn-related corrosion products are

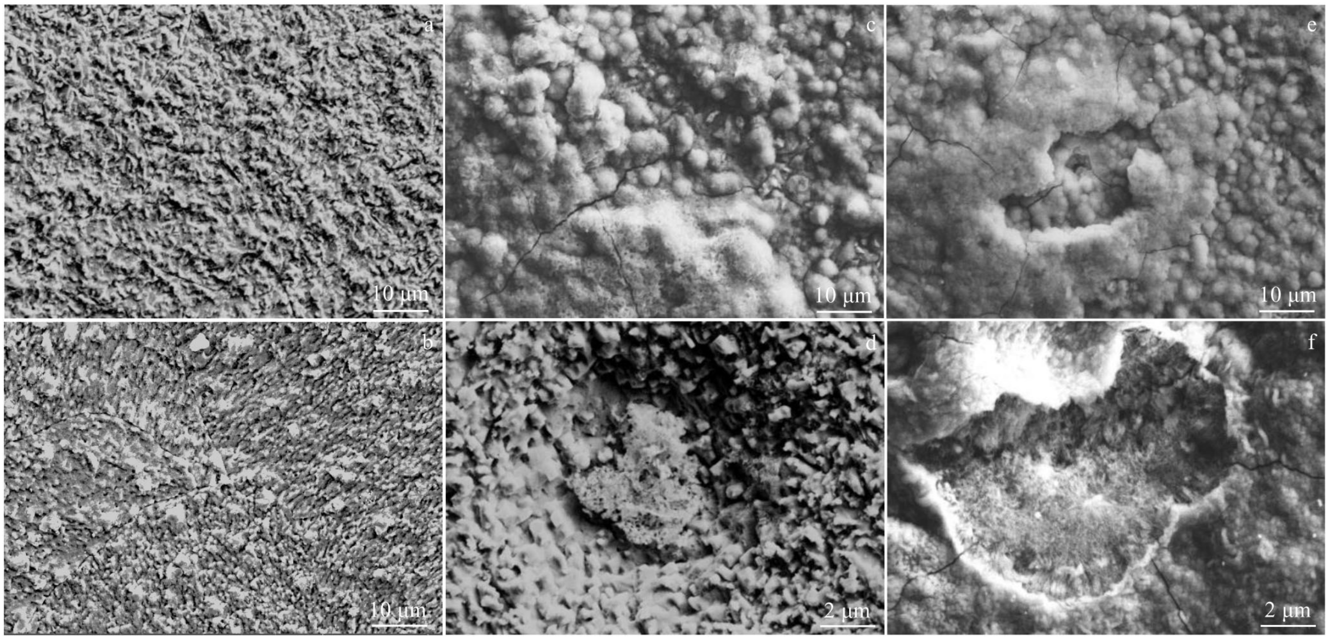

Fig.8 SEM surface morphologies of Cu-Mn cladding layer specimens with different Mn contents after electrolytic corrosion at constant potential in 3.5wt% NaCl solution for 120 min: (a–b) Mn3Cn, (c–d) Mn5Cu, and (e–f) Mn7Cu

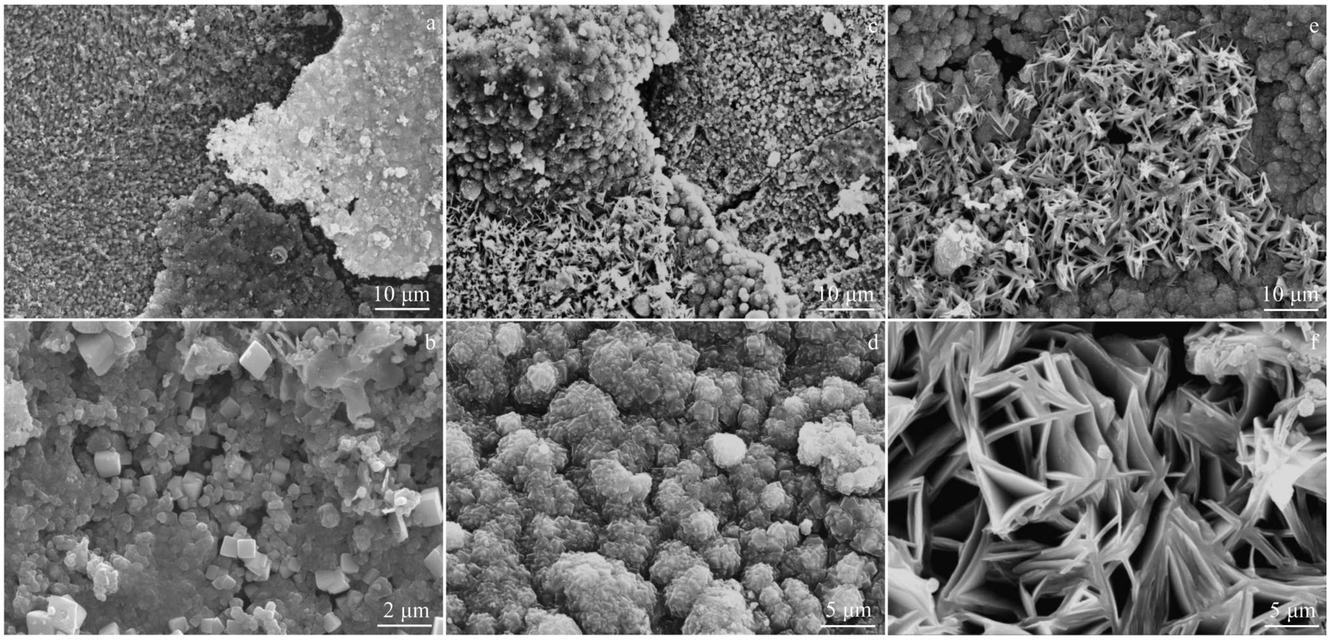

Fig.9 SEM corrosion morphologies of Mn7Cu specimen after electrolytic corrosion at constant potential for 240 min (a–b) and 360 min (c–f)

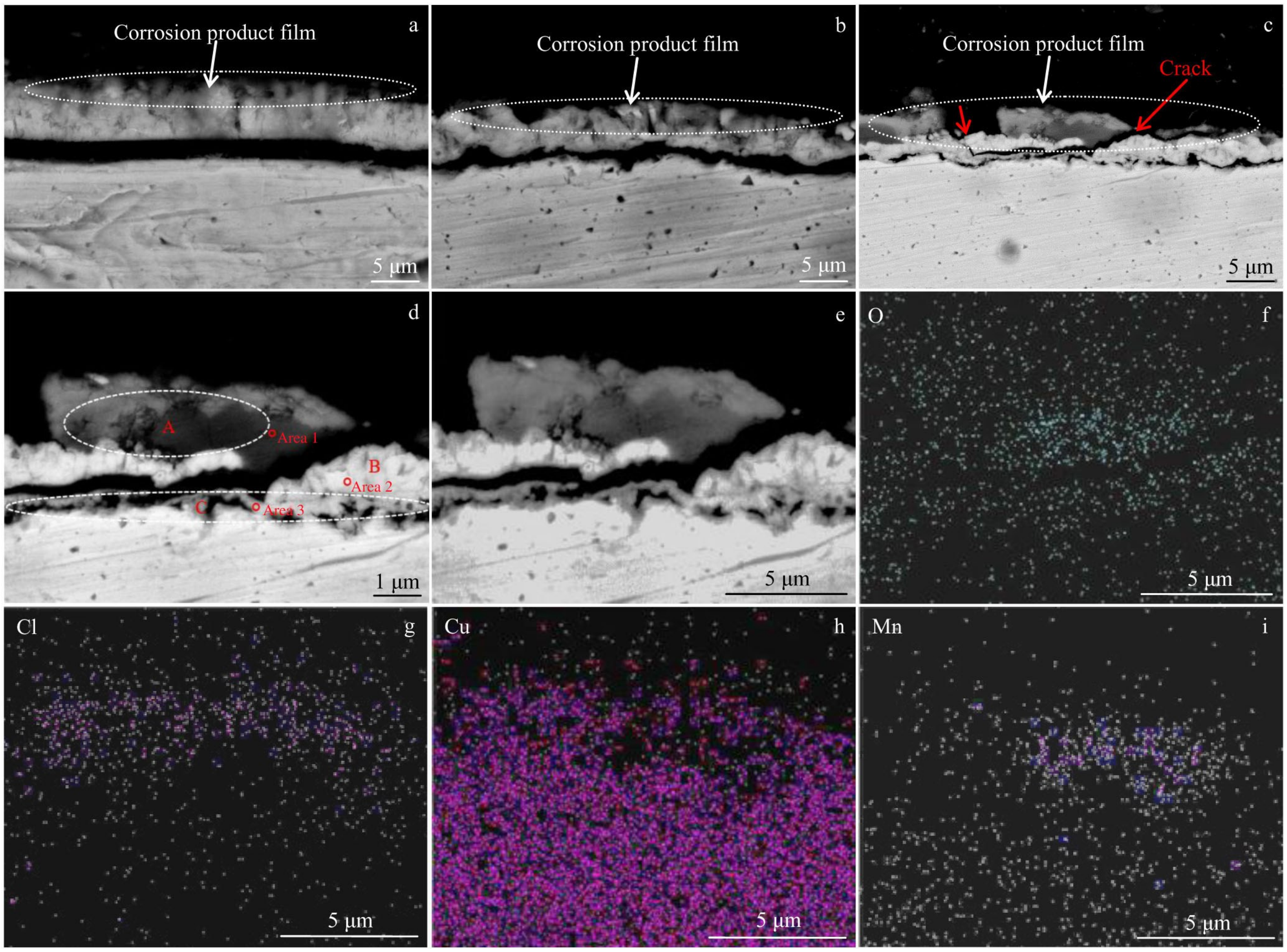

Fig.10 Cross-sectional corrosion morphologies of Mn3Cu (a), Mn5Cu (b), and Mn7Cu (c) specimens after electrolytic corrosion at constant potential; enlarged crack morphology of Fig.10c (d); SEM morphology of the corrosion product film and uncorroded cladding layer of Cu-Mn specimen (e) and corresponding EDS element distribution maps of O (f), Cl (g), Cu (h), and Mn (i) elements

Table 7 EDS analysis results of area 1, area 2, and area 3 in Fig.10d (wt%)

Area	O	Cl	Cu	Mn
1	27.8	7.2	29.8	35.1
2	12.3	2.4	84.1	1.2
3	12.8	1.6	81.8	3.8

concentrated at the outer surface. The gray laminated corrosion products are generated by the outward precipitation of Cu-Mn solid solution. As a result, the corrosion firstly occurs from the region A (Fig. 10d), then the cracks are initiated (region B in Fig. 10d), and finally the cracks become porous area (region C in Fig. 10d). The corrosion intensifies after the region A becomes loose, and the region B and region C become the outermost layer, which promotes the continuous corrosion. These cracks with longitudinal distributions promote the seawater permeation into the inner layer, and Cu_2O, $Cu_2(OH)_3Cl$, and other corrosion products cause the peeling of the outer corrosion products, thereby promoting the release of Cu^{2+} ions.

Fig. 10e shows SEM image of the corrosion product film layer and uncorroded cladding layer of Mn7Cu specimen, and the corresponding EDS element distribution maps are shown in Fig. 10f–10i. It can be seen that O and Cl elements are distributed in all corrosion products on the cladding layer. The content of O element in the outer corrosion products is slightly higher than that in the inner layer, indicating that the exterior corrosion products are mainly composed of oxides. The content of Mn element in the external corrosion product is significantly higher than that in the inner layer. The content of Cu element in the corrosion products on the outer layer is lower than that in the inner layer, suggesting that the inner layer contains more Cu corrosion products.

Table 8 shows EDS analysis results of corrosion products of Cu-Mn cladding layers with different Mn contents after accelerated electrolytic corrosion for 120 min. Table 9 shows EDS analysis results of corrosion products of Mn7Cu specimen after accelerated electrolytic corrosion for different durations. It can be seen that under the same corrosion medium, temperature, and corrosion duration, the corrosion products of Cu-Mn cladding layers with different Mn contents consist of Cu, O, Cl, and Mn elements.

Based on EDS analysis results of Table 8, it can be seen that the content of Cu, O, and Mn elements in Mn3Cu specimen is stable of about 92wt%, 5wt%, and 2wt%, respectively. The content of Cl element is only 0.15wt%. Thus, it is inferred that the main component is Cu-Mn solid solution and a small number of oxides[40]. The irregular white flake corrosion products at the exfoliation area of Mn5Cu specimen is composed of Cu (80.52wt%), Cl (6.39wt%), O (12.45wt%), and a small amount of Mn. The specimen surface layer contains partial oxides and chlorides of Cu-Mn solid solution; the inner layer is mainly composed of the chloride and oxide of Cu and it does not contain Mn.

Table 8 EDS analysis results of corrosion products on Cu-Mn cladding layer specimens with different Mn contents after electrolytic corrosion at constant potential in NaCl solution for 120 min (wt%)

Specimen	Cu	O	Cl	Mn
Mn3Cu	92.40	4.64	0.15	2.81
Mn5Cu	80.52	12.45	6.39	0.64
Mn7Cu	54.84	29.14	15.68	0.33

Table 9 EDS analysis results of corrosion products on Mn7Cu specimen after electrolytic corrosion at constant potential in NaCl solution for different durations (wt%)

Time/min	Cu	O	Cl	Mn
120	54.84	29.14	15.68	0.33
240	52.17	31.36	15.84	0.63
360	68.79	19.33	11.50	0.39

In the severely corroded Mn7Cu specimen (Table 9), the content of Cu, Cl, and O elements is 54.84wt%, 15.68wt%, and 29.14wt% , respectively; the content of Mn element is very small. It is inferred that the surface corrosion products are mainly oxides and chlorides of Cu-Mn solid solution. The O content in corrosion products at the exfoliation area and that at the outermost light gray corrosion products are slightly increased due to the generation of Cu_2O and other oxides. This result also suggests that the seawater enters through cracks and defects with the corrosion proceeding. The reaction continues in the inner layer, promoting the peeling of the outer layer of corrosion products, so the O content is relatively high at the exfoliation area. In the Cu-Mn cladding layers with different Mn contents, with increasing the Mn content, the Cu content is decreased and the O and Cl element contents are gradually increased. This result indicates that the corrosion degree is gradually deepened with increasing the Mn content, which is consistent with the previous electrochemical results. In Mn7Cu specimen, the Cu element content at the crater is increased with increasing the corrosion duration. This phenomenon indicates that at the exfoliation area, the Cu element in the inner layer leaks outward, therefore increasing the release rate of Cu ions.

Fig. 11a shows XRD patterns of corrosion products of Cu-Mn cladding layers with different Mn contents after electrolytic corrosion at constant potential for 120 min. Fig. 11b shows XRD patterns of corrosion products of Mn7Cu specimen after electrolytic corrosion at constant potential for different durations. It can be seen that after electrolytic corrosion at constant potential for 120 min, the corrosion products of Mn3Cu specimen mainly consist of Cu/Mn solid solution and Cu_2O; the corrosion products of Mn5Cu specimen mainly consist of Cu-Mn solid solution and Cu_2O; the corrosion products of Mn7Cu specimen mainly consist of Cu/Mn solid solution, Cu_2O, and $Cu_2(OH)_3Cl$. The corrosion products of Mn7Cu specimen are mainly composed of Cu/Mn solid solution, Cu_2O, $Cu_2(OH)_3Cl$, and CuCl

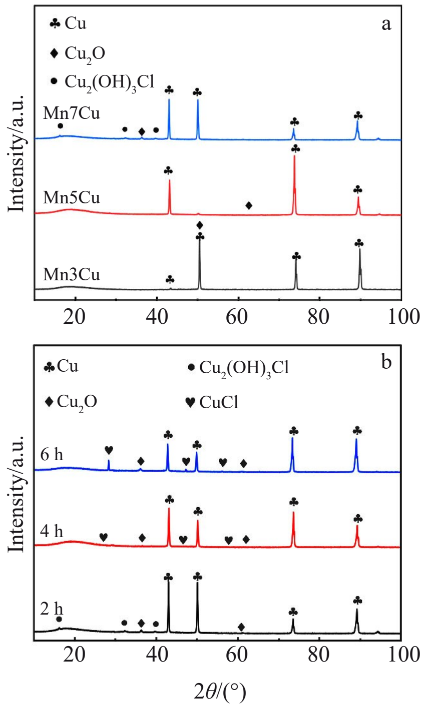

Fig.11 XRD patterns of corrosion products of different Cu-Mn cladding layers after corrosion for 120 min (a) and Mn7Cu specimen after corrosion for different durations (b)

after corrosion for 240 – 360 min, but the component contents are different.

2.7 Copper ion release rate

It is known that the copper ion release rate can be calculated based on the copper ion concentration, and the related expression is as follows:

$$R = \frac{24\left[\left(\rho_V F\right) - \rho_B\right]V}{tA} \tag{5}$$

where R is the copper ion release rate ($\mu g \cdot cm^{-2} \cdot d^{-1}$); ρ_V is the mass fraction of copper ions in the exudate ($\mu g \cdot L^{-1}$); F is the correction factor of the exudate specimen, F=1.01; ρ_B is the mass fraction of copper ions in the blank solution of artificial seawater ($\mu g \cdot L^{-1}$); V is the volume of simulated seawater solution in the exudate tank (L); t is the immersion time of the specimen in the exudate tank (h); A is the exposed surface area of the specimen (cm^2).

Fig. 12 shows the calculated copper ion release rates of Cu-Mn cladding layers with different Mn contents during continuous immersion in seawater for 45 d. It can be seen that the initial copper ion release rate is high, and the copper ion release rate is positively correlated to the Cu content in the cladding layer. The highest Cu ion release rate is achieved for Mn3Cu specimen, and Mn7Cu specimen has the relatively slow Cu ion release rate. During the corrosion for 4–45 d, for all the Cu-Mn cladding layers, the copper ion release rate firstly increases, then decreases, and finally fluctuates around a constant value. The copper ion release rate of Mn7Cu specimen is always the highest. This is probably because in the corrosion process, the Mn element can dissolve the cladding layer, thereby exposing the uncorroded area for further corrosion, as shown in Fig. 13. The higher the Mn content, the faster the corrosion rate of the cladding layer and the faster the copper ion release rate. Generally, the minimum ion release rate of 10 $\mu g \cdot cm^{-2} \cdot d^{-1}$ can inhibit hydroids corrosion, and that of 20–30 and 40–50 $\mu g \cdot cm^{-2} \cdot d^{-1}$ can hinder the jellyfish and algae corrosion, respectively. The ion release rate of at least 50 $\mu g \cdot cm^{-2} \cdot d^{-1}$ can be used to impede the bacterial mucosa. The experiment results show that the minimum copper ion release rate is 68.288 $\mu g \cdot cm^{-2} \cdot d^{-1}$ for all Cn-Mn cladding layers in this research after corrosion for 45 d, indicating that all these cladding layers can inhibit the growth of various sea creatures, and thereby achieving the anti-fouling effect.

Fig. 13 shows the schematic diagram of the corrosion process of Cu-Mn cladding layers in 3.5wt% NaCl solution. Adding Mn can promote the growth of cracks and defects on the cladding layer surface. The seawater enters the material through the cracks, which results in the peeling of corrosion products and promotes the stable release of Cu^{2+} ions. The higher the Mn content, the more the corrosion cracks, the easier the peeling of corrosion products, and the

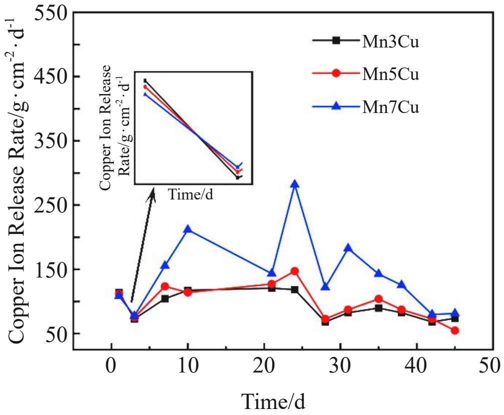

Fig.12 Copper ion release rate of Cu-Mn cladding layers with different Mn contents

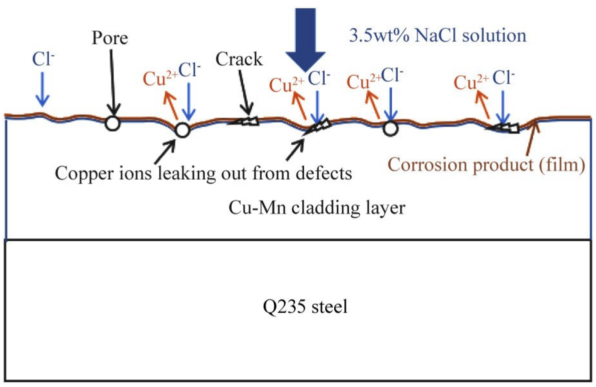

Fig.13 Schematic diagram of corrosion mechanism of Cu-Mn cladding layer in 3.5wt% NaCl solution

faster the Cu^{2+} ion release rate.

3 Conclusions

1) The Cu-Mn cladding layer with 3wt% Mn (Mn3Cu specimen) has a more positive open circuit potential, and Cu-Mn cladding layer with 7wt% Mn (Mn7Cu specimen) has a more negative open circuit potential. Thus, the Mn3Cu specimen has better corrosion resistance. The corrosion current density of Mn3Cu specimen is the smallest, whereas that of Mn7Cn specimen is the largest, indicating that Mn7Cu specimen has higher corrosion tendency. The Mn3Cu specimen has the largest capacitive arc radius, and the Mn7Cu specimen has the smallest capacitive arc radius, which also suggests that Mn7Cu specimen has higher corrosion tendency. Additionally, with increasing the Mn content, the corrosion resistance of Cu-Mn cladding layer is decreased.

2) During the salt spray corrosion cycle, the corrosion degree of the cladding layers is increased with increasing the Mn content, and the average mass loss of Mn7Cu specimen is the largest, which is 1.20 times higher than that of Mn3Cu specimen.

3) After the accelerated corrosion by electrolysis, with increasing the Mn content, the corrosion products on the surface of cladding layer are gradually changed from relatively dense products and flat gray flakes/layers into the loose products with cracks and pits. The Mn element in the cladding layer promotes the corrosion and its corrosion products can be combined with Cu-related corrosion products, which accelerates the loosening of Cu-related corrosion products. With the corrosion proceeding, the surface corrosion product of Cu-Mn cladding layers is gradually loosened, the cracks slowly grow, and therefore the pits are formed. The Cu element is concentrated at the pits, and the Cu ions in the inner layer are leached outward, thereby increasing the release rate of Cu ions.

4) The Cu-Mn cladding layers with different Mn contents can inhibit the growth of all sea creatures, thereby achieving the anti-fouling effect. The higher the Mn content in the cladding layer, the faster the copper ion release rate.

References

1 Deng Dewei, Zheng Haitong, Ma Zhandong *et al*. *Journal of Functional Materials*[J], 2020, 51(6): 6001 (in Chinese)

2 Kong Y, Liu Z D, Li B. *Rare Metal Materials and Engineering*[J], 2021, 50(8): 2694

3 Zhao Jiuyi. *Special Casting & Nonferrous Alloys*[J], 2006, 26(6): 390 (in Chinese)

4 Li Cong, Li Mingzhao, Wang Yueqi *et al. Rare Metal Materials and Engineering*[J], 2011, 40(1): 156 (in Chinese)

5 Ren L, Cheng Y H, Wang Q H *et al*. *Colloids and Surfaces A*[J], 2020, 591: 124 502

6 Chasse K R, Scardino A J, Swain G W. *Progress in Organic Coatings*[J], 2020, 141: 10 555

7 Rajesh R, Kulkarni M V, Vergis B R *et al. Materials Today: Proceedings*[J], 2022, 49(3): 703

8 Drach A, Tsukrov I, DeCew J *et al. Corrosion Science*[J], 2013, 76: 453

9 Liu B S, Wang Y N, Zhang Y Z *et al. Rare Metal Materials and Engineering*[J], 2021, 50(1): 49

10 Sugimoto, K, Hoshino K, Kageyama M *et al. Corrosion Science*[J], 1975, 15(6–12): 709

11 Ma Conghui, Wang Changjun, Shen Tao *et al*. *Heat Treatment of Metals*[J], 2020, 45(8): 97 (in Chinese)

12 Huang Yongchang, Jin Xiaodong. *Corrosion & Protection*[J], 1990, 11(2): 90 (in Chinese)

13 Chang T, Herting G, Goidanich S *et al. Corrosion Science*[J], 2019, 149: 54

14 Chang T, Maltseva A, Volovitch P *et al. Corrosion Science*[J], 2020, 166: 108 477

15 Cheng Ji. *Special Casting & Nonferrous Alloys*[J], 1991, 11(4): 33 (in Chinese)

16 Niu C N, LaRosa C R, Miao J S *et al. Nature Communications*[J], 2018, 9(1): 1363

17 Christofidou K A, Pickering K J, Orsatti P *et al. Intermetallics*[J], 2018, 92: 84

18 Bracq G, Laurent-Brocq M, Perrière L *et al. Acta Materialia*[J], 2017, 128(15): 327

19 Kai W, Li C C, Cheng F P *et al. Corrosion Science*[J], 2016, 108: 209

20 Gu Yu, Dong Changsheng, Ma Mingxing *et al. Acta Metallurgica Sinica*[J], 2011, 47(3): 349 (in Chinese)

21 Zheng Jiwei, Zhang Shichao, Liu Wenbo *et al. Hot Working Technology*[J], 2011, 40(24): 40 (in Chinese)

22 Zhang Rongwei, Sun Junwei, Li Shengyan *et al. Nonferrous Metals Science and Engineering*[J], 2018, 9(4): 60 (in Chinese)

23 Pardo A, Merina M C, Coy A E *et al. Corrosion Science*[J], 2008, 50(6): 1796

24 An L C, Cao J, Wu L C *et al. Journal of Iron and Steel Research International Volume*[J], 2016, 23(12): 1333

25 Kong D C, Dong C F, Ni X Q *et al. npj Materials Degradation*[J], 2019, 3(1): 24

26 Cai Y C, Chen Y, Lou Z *et al. Materials & Design*[J], 2017, 133: 91

27 Singh S, Singh P, Singh H *et al. Materials Today: Proceedings*[J], 2019, 18(3): 830

28 Ramachandran S, Lakshminarayanan A K. *Transactions of Nonferrous Metals Society of China*[J], 2020, 30(3): 727

29 Tang C H, Cheng F T, Man H C. *Surface and Coatings Technology*[J], 2004, 182(2–3): 300

30 Fan Xuehua, Yu Yong, Zhang Ziru *et al. Surface Technology*[J], 2020, 49(7): 287 (in Chinese)

31 Wang X W, Wang W, Chen W *et al. Journal of Materials Science & Technology*[J], 2022, 98: 219

32 Giuliani L, Tamba A, Modena C. *Corrosion Science*[J], 1971, 11(7): 485

33 Horton D J, Ha H, Foster L L *et al. Electrochimica Acta*[J], 2015, 169: 351

34 Chen Qingjun, Jiang Wei, Zhang Fabi *et al. Rare Metal Materials and Engineering*[J], 2016, 45(9): 2322 (in Chinese)

35 Chen Hu, Zhou Hao, Wang Shuli *et al. Corrosion & Protection*[J], 2018, 39(12): 936 (in Chinese)

36 Nyby C, Guo X L, Saal J E *et al. Scientific Data*[J], 2021, 8(1): 58

37 Yang X T, Zeng R, Fu X Y *et al. Corrosion Science*[J], 2022, 205: 110 408

38 Li B Z, Ouyang Y B, Haider Z *et al. Colloids and Surfaces A*[J], 2021, 616: 126 337

39 Ekerenam O O, Ma A L, Zheng Y G *et al. Journal of Materials Engineering and Performance*[J], 2017, 26(4): 1701

40 Sun Tingting, Li Ning, Xue Jianjun *et al. Equipment Environmental Engineering*[J], 2010, 7(4): 25 (in Chinese)

不同Mn含量Cu-Mn合金熔覆层的腐蚀特性

齐英男，刘宗德，谢瑞祥，马荷蓉，宁华清

(华北电力大学 电站能量传递转化与系统教育部重点实验室，北京 102206)

摘　要：为研究不同Mn含量Cu-Mn合金熔覆层的腐蚀特性和防污性能，利用激光熔覆技术制备了成分均匀、稀释率低的Cu-Mn合金熔覆层。采用电化学测试、盐雾腐蚀实验、腐蚀形貌观察及铜离子释放试验对3种不同Mn含量的Cu-Mn合金熔覆层在3.5%（质量分数）NaCl溶液中的腐蚀特性进行研究，重点研究了Mn对腐蚀产物和铜离子释放率的影响。结果表明：在电化学测试中，随着Mn含量增多，熔覆层的耐腐蚀性降低。盐雾腐蚀实验中，随着Mn含量的增多，Cu-Mn合金熔覆层腐蚀程度加深，平均质量损失增大。对电解腐蚀后的熔覆层样品进行腐蚀形貌观察，Mn含量高的Cu-Mn合金样品生成的腐蚀产物较低Mn含量的样品更疏松，裂纹孔洞数量多，腐蚀产物更易剥落。铜离子释放试验中，3种Mn含量合金熔覆层样品都可以抑制海洋生物生长，且Mn含量越高，铜离子渗出率越大，在防污材料方面有良好的应用前景。

关键词：Cu-Mn合金；激光熔覆；电化学；盐雾腐蚀；腐蚀形貌；铜离子

作者简介：齐英男，男，1996年生，硕士，华北电力大学电站能量传递转化与系统教育部重点实验室，北京 102206，电话：010-61772277，E-mail：67849123@qq.com